Near-Ambient Pressure XPS and NEXAFS Study of a Superbasic Ionic Liquid with CO_2

Jordan Cole[*,†], *Zoë Henderson*[†,#], *Andrew G. Thomas*[‡], *Claudia L. Compeán-González*[‡], *Adam J. Greer*[‖], *Christopher Hardacre*[‖], *Federica Venturini*[§], *Wilson Quevedo Garzon*[§,⊥], *Pilar Ferrer*[§], *David C. Grinter*[§], *Georg Held*[§], *and Karen L. Syres*[*,†]

† Jeremiah Horrocks Institute for Mathematics, Physics and Astronomy, University of Central Lancashire, Preston, PR1 2HE, UK

‡ Department of Materials Science, Photon Science Institute and Henry Royce Institute, University of Manchester, Manchester, M13 9PL, UK

‖ Department of Chemical Engineering and Analytical Science, University of Manchester, Manchester, M13 9PL, UK

§ Diamond Light Source, Didcot, OX11 0DE, UK

Keywords: ionic liquids, x-ray photoelectron spectroscopy, gas capture, thin films, density functional theory.

*Email: KSyres@uclan.ac.uk; JCole4@uclan.ac.uk

ABSTRACT

In situ photoemission and near edge X-ray absorption fine structure (NEXAFS) techniques have been used to study the interaction of CO_2 with an ionic liquid thin film. A thin film of the superbasic ionic liquid (SBIL) trihexyltetradecylphosphonium benzimidazolide ($[P_{66614}][benzim]$) was prepared on a rutile TiO_2 (110) surface and exposed to CO_2 at near-ambient pressures. NEXAFS measurements combined with density functional theory calculations indicate a realignment of $[benzim]^-$ anions from 27° from the surface normal to 54° upon exposure to CO_2. Angle-resolved X-ray photoelectron spectroscopy (AR-XPS) shows evidence of irreversible CO_2 absorption in thin films of $[P_{66614}][benzim]$ and a greater concentration of CO_2-reacted anions in the deeper layers. These results give a new perspective on CO_2 uptake in ionic liquids and fundamental interactions at the liquid-gas interface. Understanding this interfacial behaviour is important for developing ILs for gas capture applications and may influence the performance of other IL-based technologies.

INTRODUCTION

Carbon dioxide (CO_2) capture and separation has become an important process in reducing CO_2 emissions in fossil fuel-fired power plants. In current industrial applications, alkanolamine solvents such as monoethanolamine (MEA) are typically used for CO_2 capture but incur unwanted long-term costs due to the energy required to regenerate them.[1] In recent years, ionic liquids (ILs) have been researched as potential green alternatives for CO_2 capture in post-combustion power plants owing to their high CO_2 capacity, very low volatility, high thermal stability and lower regeneration temperatures compared to MEA.[2–4]

ILs consist of anions and cations held together by Coulombic forces and have lower melting points than conventional ionic salts due to the bulky and unsymmetrical nature of the ions.[5] The vast number of possible anion-cation combinations allows for the physical and chemical properties of an IL to be fine-tuned.[6] As well as the properties discussed above, ILs have wide electrochemical windows and can have a low corrosivity and toxicity.[6,7] Their numerous, varied, and tuneable properties make ILs promising for a wide range of potential applications including electrolytes for electrochemical devices and nanostructure growth,[8–10] solar cell fabrication and performance improvement,[11,12] and the capture and separation of environmentally harmful gases such as CO_2 and SO_2.[13,14] A recent sub-group of ILs called superbasic ILs (SBILs) are being researched for gas capture applications due to their higher CO_2 capacities and low viscosity increases compared to conventional ILs.[15] SBILs consist of quaternary phosphonium/ammonium-based cations paired with a superbasic anion such as imidazolide, triazolide or phenoxide.[16,17]

There is little information available in the literature about monolayer and multilayer behaviour of SBILs. Monolayer/multilayer behaviour of conventional imidazolium-based ILs has been investigated using thin and ultrathin IL depositions on a number of substrates in vacuo, including

glass,[18] mica,[19] gold,[20] and nickel.[21] ILs are more highly structured than most molecular liquids, and these studies have all revealed vital information pertaining to the layering and stacking behaviour of these ILs. However, there is little available literature involving the use of X-ray absorption techniques, specifically near edge X-ray absorption fine structure (NEXAFS) spectroscopy. NEXAFS can be used to quantitatively determine the orientation of aromatic IL ions at submonolayer, monolayer, and multilayer coverages.[22] Using near-ambient pressure synchrotron facilities it is now possible to conduct XPS and NEXAFS measurements of liquid-gas interfaces. It is also common to pair experimental NEXAFS with density functional theory (DFT) simulations due to a lack of comparable experimental spectra. No literature currently exists in the way of NEXAFS investigations of IL/gas systems under near-ambient pressure conditions, so simulated NEXAFS spectra will be used in our study to provide further insight into our experimental results.

Herein, we report a combined *in situ* XPS and NEXAFS study into the ordering and interactions of a multilayer thin film deposition of the SBIL $[P_{66614}]$[benzim] on rutile TiO_2 (110) before, during, and after exposure to CO_2. NEXAFS measurements are compared to simulated NEXAFS spectra calculated using DFT and quantum chemical simulations are used to visualise the unoccupied antibonding molecular orbitals. This combined approach identifies chemical reactions at the ionic liquid/gas interface and reordering of the ionic liquid upon exposure to gas.

EXPERIMENTAL AND THEORETICAL METHODS

Experimental measurements of the IL trihexyltetradecylphosphonium benzimidazolide ($[P_{66614}]$[benzim]) were carried out at beamline VerSoX (B07) at Diamond Light Source in the UK (photon energy range 250 - 2800 eV).[23] The $[P_{66614}]^+$ cation was synthesised using a trihexylphosphine precursor as detailed in ref. [24]. The VerSoX endstation has a hemispherical

PHOIBOS 150 NAP electron energy analyser and the analysis chamber is backfilled with gas to carry out near-ambient pressure measurements. The angle of the sample can be rotated with respect to the analyser whilst at near-ambient pressure which allows angle-resolved NEXAFS measurements. A rutile TiO_2 (110) single crystal (PI-KEM) was cleaned via Ar^+ sputter/anneal cycles (sputtering at 1 keV for 10 minutes and annealing at 700°C for 10 minutes) until XPS spectra showed no contamination. Then, a 0.5 M solution of $[P_{66614}]$[benzim] (chemical structure shown in Figure 1(a)) in methanol was deposited dropwise via a syringe onto the rutile TiO_2 (110) single crystal in the load lock of the end station in ambient laboratory conditions. It was then allowed to degas for several hours under vacuum conditions prior to measurements.

Near-ambient pressure XPS (NAP-XPS) measurements of the $[P_{66614}]$[benzim] multilayer thin film were taken at high vacuum (as presented), during exposure to three different pressure regimes of CO_2 (10^{-6} mbar, 1 mbar, and 5 mbar), and following exposure to CO_2 (after the gas was pumped out). The reaction of CO_2 with the $[benzim]^-$ anion is shown in Figure 1(a). XPS scans across the IL layer showed a film with inhomogeneous thickness, therefore measurements were taken on a very thin part of the film such that the Ti 2p signal from the TiO_2 substrate was still detectable (homogeneous over approximately 2 mm square, approximately 0.5 nm thick on average). The sample was moved approximately 0.2 mm between scans to avoid degradation and charging of the film (beam size $\leq$ 200 μm × $\leq$ 200 μm). All XPS peaks have been fitted using a Gaussian-Lorentzian product line shape (30:70 Lorentzian:Gaussian contribution) and a linear background, using the software CasaXPS.[25] The binding energy scale for all regions has been calibrated to the alkyl C 1s signal at 285.0 eV and all fitted peaks are quoted to ± 0.1 eV binding energy.[26]

The photoemission measurements were accompanied by *in situ* C K edge and N K edge NEXAFS. C K edge NEXAFS spectra were recorded over the range 280 to 315 eV by monitoring

the C Auger peak at a kinetic energy of 260 eV. N K edge NEXAFS spectra were recorded over the range 390 to 430 eV by monitoring the N Auger peak at a kinetic energy of 375 eV. The NEXAFS spectra are intensity-normalised such that the step between 280 eV and 315 eV (for the C K edge), and between 390 eV and 430 eV (for the N K edge), is equal to unity. Background correction procedures are shown in the Supporting Information (SI).

The experimental NEXAFS spectra are compared to theoretical spectra obtained using DFT simulations performed in the software StoBe-deMon.[27] The isolated [benzim]$^-$ anion was geometry optimised in Avogadro (version 1.2) before excited state calculations were carried out in StoBe-deMon.[28] For the C K edge, theoretical NEXAFS spectra were obtained for each carbon atom in the anion and then combined to produce the total theoretical spectrum for the anion. The same procedure was carried out for the N K edge, using each nitrogen atom in the anion. These simulations represent an angular average in which the anions are considered to be randomly oriented with respect to the incoming electric field vector. The spectra were then broadened using Gaussian functions with linearly increasing Full-Width at Half Maxima (FWHM) from 0.7 eV to 12.0 eV between the photon energies of 290 and 310 eV. This accounts for the reduced lifetime of the σ* resonances.[29] The theoretical NEXAFS spectra for each individual atom were energy calibrated by calculating the difference in total energy between the ground state and first core-excited state. This gives the energy of the first transition in the NEXAFS spectrum for that atom. The calibrated individual spectra were added together to produce the total theoretical spectra. The total theoretical spectra were then simply shifted in energy to match the experimental NEXAFS spectra. To complement NEXAFS simulations, unoccupied molecular orbitals were calculated using the software ORCA (version 4.0) and visualised using Avogadro.[30,31]

RESULTS AND DISCUSSION

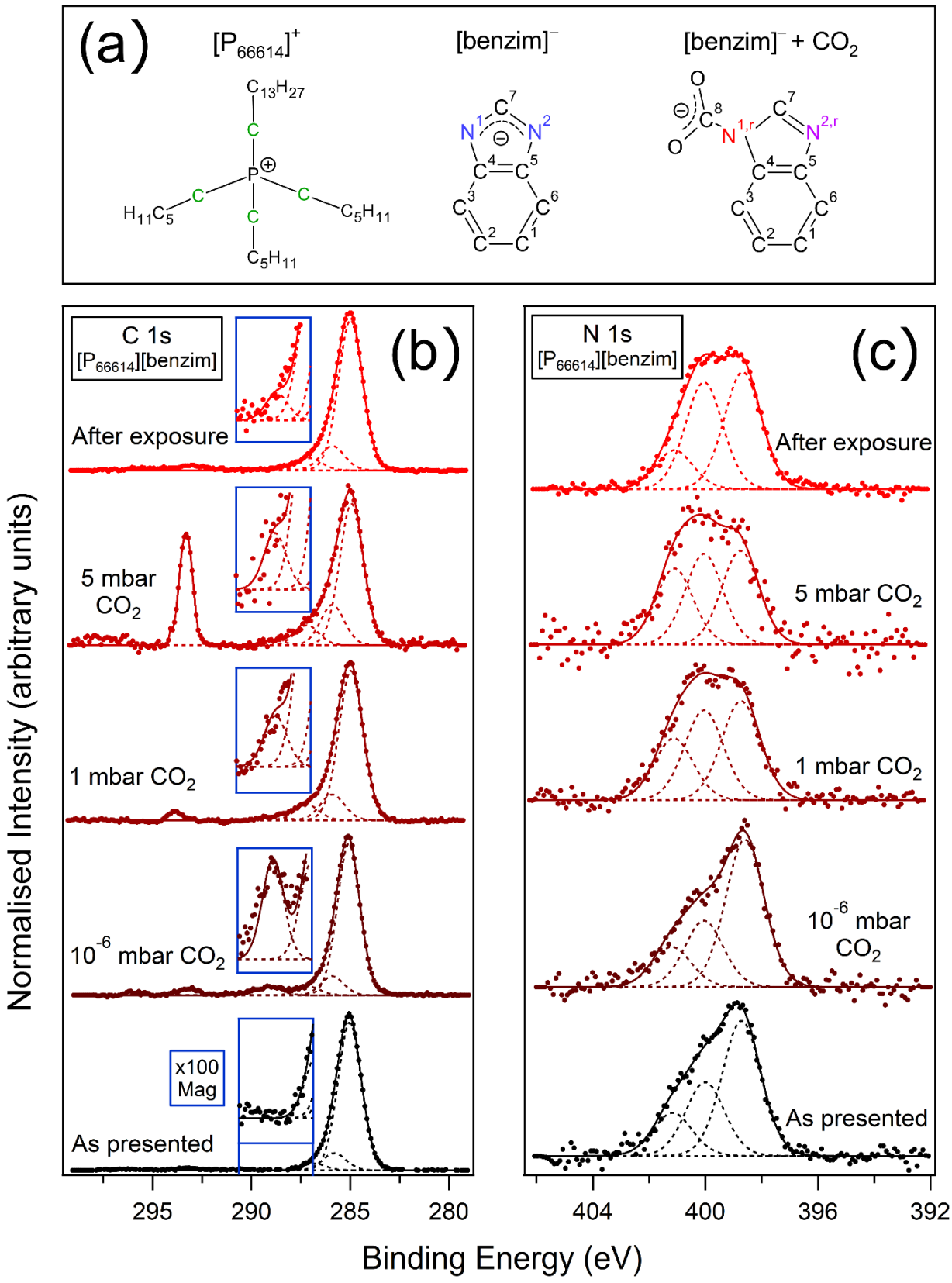
(a)
[P66614]+
[benzim]−
[benzim]− + CO2
(b)
C 1s
[P66614][benzim]
After exposure
5 mbar CO2
1 mbar CO2
10-6 mbar CO2
x100 Mag
As presented
(c)
N 1s
[P66614][benzim]
After exposure
5 mbar CO2
1 mbar CO2
10-6 mbar CO2
As presented
Normalised Intensity (arbitrary units)
295
290
285
280
404
400
396
392
Binding Energy (eV)

Figure 1. (a) Chemical structure of the $[P_{66614}]^+$ cation with C_{hetero} atoms highlighted in green and $C_{aliphatic}$ in black. The $[benzim]^-$ anion is shown as presented and while reacted with CO_2, where $N^{1,r}$ (red) and $N^{2,r}$ (purple) denote the N atoms following reaction with CO_2 at the N^1 site. (b) C 1s and (c) N 1s XPS regions recorded at photon energies of 585 eV and 700 eV, respectively, for a thin film of $[P_{66614}][benzim]$ as presented, exposed to 10^{-6} mbar CO_2, 1 mbar CO_2, 5 mbar CO_2, and after exposure. The C 1s binding energy range between 287 to 291 eV is magnified × 100 (blue boxes) and shows the formation of a carbamate peak upon absorption of CO_2.

NAP-XPS measurements of multilayer $[P_{66614}][benzim]$ were taken upon exposure to increasing pressures of CO_2 (10^{-6}, 1 and 5 mbar) in the C 1s, N 1s, and P 2p regions (taken at photon energies of 585, 700, 830, and 430 eV, respectively). The fitted components of these regions are summarised in Table S1 of the SI, and the survey spectra for each exposure stage are shown in Figure S1. The Ti 2p spectra remain relatively unchanged throughout the exposure regime and simply result from Ti atoms in the TiO_2 substrate. The Ti 2p region is, therefore, shown in Figure S2.

All the spectra in the C 1s region shown in Figure 1(b) are normalised to the main peak which can be fitted with two components attributed to carbon atoms in the $[P_{66614}]^+$ cation. The component at 285.0 eV is attributed to aliphatic carbon ($C_{aliphatic}$, see Figure 1(a)) and the component at 285.9 eV is attributed to carbon atoms immediately around the phosphorous atom, C_{hetero}. Their positions are consistent with previous reports for phosphonium-based ILs with the same $[P_{66614}]^+$ cation.[26] For the IL as presented, the area ratio of these components ($C_{aliphatic}$:C_{hetero}) is 8.6:1 compared to 7:1 from the stoichiometry of the cation. The slight discrepancy from stoichiometry may be due to aliphatic contamination during deposition of the IL in atmosphere or could be due to photoelectron diffraction effects. It is possible that C−C bonds in the $[benzim]^-$

anion provide a small contribution to the main $C_{aliphatic}$ peak which can also affect this $C_{aliphatic}$:C_{hetero} ratio. As discussed in our P 2p analysis below, there will also be aliphatic and hetero contributions from the trihexylphosphine precursor used in the synthesis of the IL at similar BEs. The C 1s peak is asymmetric towards higher binding energies (BEs) and can be fitted with a component at 286.8 eV attributed to C−N bonds in the $[benzim]^-$ anion (C_{anion}).[22,26,32] Surface-sensitive grazing emission (GE, 40° from normal emission) measurements in Figure S4 suggest these three species are equally distributed throughout the thin film before exposure to CO_2.

When the IL is exposed to CO_2, it results in a peak at 293.3 eV attributed to gas-phase CO_2. This is only visible in the 1 mbar and 5 mbar exposure stages. At 10^{-6} mbar, a feature appears at a similar BE but is assigned to K 2p as discussed in the SI (Figure S4). Further changes arise when CO_2 is introduced; while the $C_{aliphatic}$ and C_{hetero} components remain unchanged in position, the C_{anion} component experiences an upward chemical shift of 0.3 eV to 287.1 eV, true for each of the pressures tested. Even after exposure to CO_2 this component remains shifted to a higher BE. Additionally, the absorption of CO_2 results in another peak at a BE of 289.0 eV, assigned to the formation of carbamate as shown in Figure 1(a). The position of this carbamate peak is in line with previous reports of CO_2 absorption in bulk coverages of $[P_{66614}][benzim]$.[33] For the IL as presented there is no carbamate peak, further confirming that this peak is due to the IL's reaction with CO_2. The region between 287 to 291 eV in Figure 1(b) is magnified (×100) to highlight the relative change in intensity of this carbamate feature with increasing CO_2 pressure. Even at pressures as low as 10^{-6} mbar of CO_2, the formation of carbamate can be observed. In fact, the carbamate peak is more intense for 10^{-6} mbar than for any of the higher pressures. At this low pressure, reactions are likely to occur at the surface, causing the intense carbamate peak. The decrease in intensity of the carbamate peak at higher pressures suggests that the saturated anions are reorienting towards

the bulk. Interestingly, this carbamate peak is still present after exposure to CO_2, implying that the absorption/desorption of CO_2 is not fully reversible in this experiment. It has been shown that bulk thicknesses of [P_{66614}][benzim] absorb and desorb CO_2 reversibly when the surrounding CO_2 gas is pumped out,[33] or when the IL is heated,[17] so it is unclear why the reaction is not fully reversible here. The thickness of the IL film is likely to influence the reversibility of reactions as discussed further in the paper.

There is a gradual shift of the carbamate peak from 289.1 eV in the 10^{-6} mbar stage to 288.8 eV after exposure. The cause of this BE shift is unknown. However, the N 1s and P 2p spectra below show significant changes throughout the exposure stages and after exposure. For example, the P 2p spectra in Figure 2 indicate reordering of a number of different species through the sample depth (as discussed further in the paper), all of which can interact with anions. These intermolecular interactions may change when the anions reorientate upon exposure to (or removal of) CO_2 and may cause a BE shift in the carbamate component after exposure.

The N 1s spectra in Figure 1(c) have been normalised to the total area and can be fitted with three components at 398.6, 400.0 and 401.1 eV. These are attributed to the chemically equivalent imidazolide N^1 and N^2 atoms ($N^{1,2}$), $N^{2,r}$ in the CO_2-reacted anion, and $N^{1,r}$ in the CO_2-reacted anion, respectively. N^1 and N^2, shown in Figure 1(a), are chemically equivalent due to resonance effects in the anion.[33,34] Imidazole carbamate forms at $N^{1,r}$ and the remaining unreacted N in the anion is labelled $N^{2,r}$. We would expect $N^{1,2}$ to be the only component in the as presented (pre-exposure) stage, however, we still see $N^{1,r}$ and $N^{2,r}$ reaction peaks. These occur from reaction to ambient CO_2 in the atmosphere when the sample was transferred to the UHV chamber. GE spectra in Figure S5 suggest that there is a greater concentration of unreacted anions ($N^{1,2}$) in the surface layers of the IL, and a greater concentration of reacted anions ($N^{1,r}$ and $N^{2,r}$) in the bulk. Similar

behaviour was reported for aqueous MEA solutions treated with CO_2 by Lewis et al., revealing that reacted MEA had a greater concentration in the bulk of the solution while unreacted MEA was more concentrated at the surface.[35]

As the IL is exposed to CO_2, the $N^{1,r}$ and $N^{2,r}$ components in Figure 1(c) increase in intensity with increasing pressure of CO_2 relative to $N^{1,2}$, further suggesting that these components are attributed to the absorption of CO_2. However, the $N^{1,r}$ and $N^{2,r}$ components deviate from the expected 1:1 area ratio. The $N^{2,r}$ component remains of comparable intensity to $N^{1,2}$, however, the $N^{1,r}$ component reduces in relative intensity compared to $N^{1,2}$. This deviation from a 1:1 area ratio may be due to the weak interaction between unreacted anions and CO_2 trapped between the IL layers. Such an interaction is likely to result in a shift of the $N^{1,2}$ component towards higher BEs, causing an apparent increase in the $N^{2,r}$ component. After exposure, the intensities of these components do not return to their pre-exposure intensities (as presented stage), indicating an irreversible reaction. The presence of reacted species both before and after exposure indicates that CO_2 cannot be fully removed by pumping down to high vacuum.

Alongside the C 1s and N 1s spectra, O 1s spectra in Figure S3 of the SI also show evidence of irreversible CO_2 absorption occurring in our thin film of $[P_{66614}]$[benzim]. The results presented, herein, suggest that the reversibility of CO_2 absorption is not only dependent on the structure of the IL, but also the thickness of the IL film. The interaction of the substrate and vacuum with our ultra-thin film of an imidazolide-based IL results in highly structured IL layers which have the potential to trap CO_2. This trapped CO_2 may impact the reversibility of CO_2 absorption in thin films with only several layers.

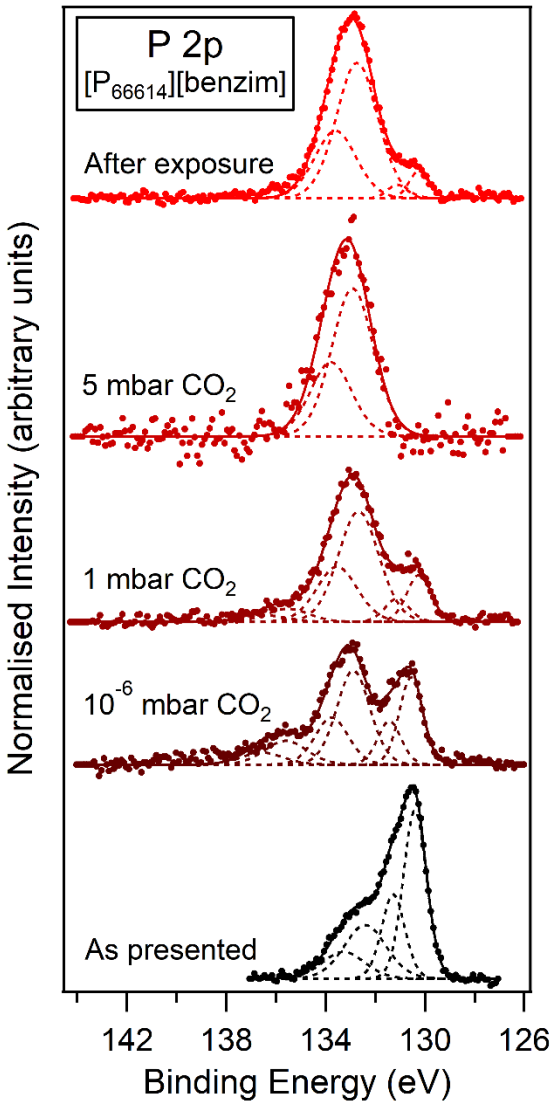

Figure 2. P 2p region recorded at a photon energy of 430 eV for multilayer $[P_{66614}][benzim]$ as presented, while exposed to various pressures of CO_2, and after exposure.

The P 2p spectra in Figure 2 have been normalized to the total area. For the as presented spectrum, the lower-energy feature can be fitted with $2p_{3/2}$ and $2p_{1/2}$ components at 130.4 and 131.3 eV and may be attributed to trihexylphosphine (THP). There is no evidence of beam damage-induced degradation of the $[P_{66614}]^+$ cation, therefore, it is likely that THP is present as a precursor impurity from the synthesis of $[P_{66614}]^+$.[24] The higher-energy feature is fitted with $2p_{3/2}$ and $2p_{1/2}$

components at 132.4 and 133.3 eV, respectively, and is assigned to the $[P_{66614}]^+$ cation.[26] The GE study in Figure S6 shows a higher concentration of THP in the bulk and a higher concentration of cations at the surface before exposure to CO_2.

Upon exposure to CO_2, the $[P_{66614}]^+$ components shift by 0.4 eV to higher BEs of 132.8 and 133.7 eV, respectively. In addition, the THP feature reduces in intensity with CO_2 exposure. These changes could be explained by a reversible reaction between phosphine (THP) and CO_2. As CO_2 exposure is increased, there is a reduction in the THP feature and an increase in the THP-CO_2 adduct feature, which is likely to occur at a similar BE to the $[P_{66614}]^+$ feature. Therefore, the $[P_{66614}]^+$ feature at about 133 eV appears to broaden and increase in intensity. The THP peak reduces to zero upon exposure to the highest pressure of 5 mbar CO_2. The THP peak reappears after exposure to CO_2 but the region is dominated by the $[P_{66614}]^+$ peak. The intensities of these two peaks are flipped compared to the IL pre-exposure peaks and may be indicative of reordering of the depth profile of the ions, or weak interaction between the cation and trapped CO_2 in the IL layers. A shoulder at 136 eV appears when the IL is exposed to low pressures of CO_2 (10^{-6} and 1 mbar), assigned as phosphine oxide, forming from the reaction between phosphine and residual water in the chamber or on the sample surface.[36] As shown in Figure S6, this phosphine oxide peak is more pronounced at GE, suggesting it is a surface phenomenon. This may explain why the peak only occurs at low pressures of CO_2, because the residual water is likely to be displaced away from the surface with increasing pressures of CO_2. Phosphine oxide should appear in the O 1s spectra but this has not been specifically assigned due to the complex nature of the O 1s region.

Angle-resolved NEXAFS of the multilayer $[P_{66614}]$[benzim] film was taken over the C K edge at X-ray incidence angles of 44° and 79° from the substrate surface as shown in Figure 3(a). This was carried out for the IL as presented and upon exposure to 1 mbar of CO_2, in order to investigate

IL orientational ordering at the surface. The IL + 1 mbar CO_2 spectra were divided by a gas-phase CO_2 NEXAFS spectrum recorded over the same photon energy range. This removed dips in the spectra due to the absorption of incoming X-rays by the surrounding CO_2 gas in the analysis chamber. However, a slight mismatch between data causes spikes to be introduced into the σ* region of the spectra, as shown in Figure S8 in the SI.

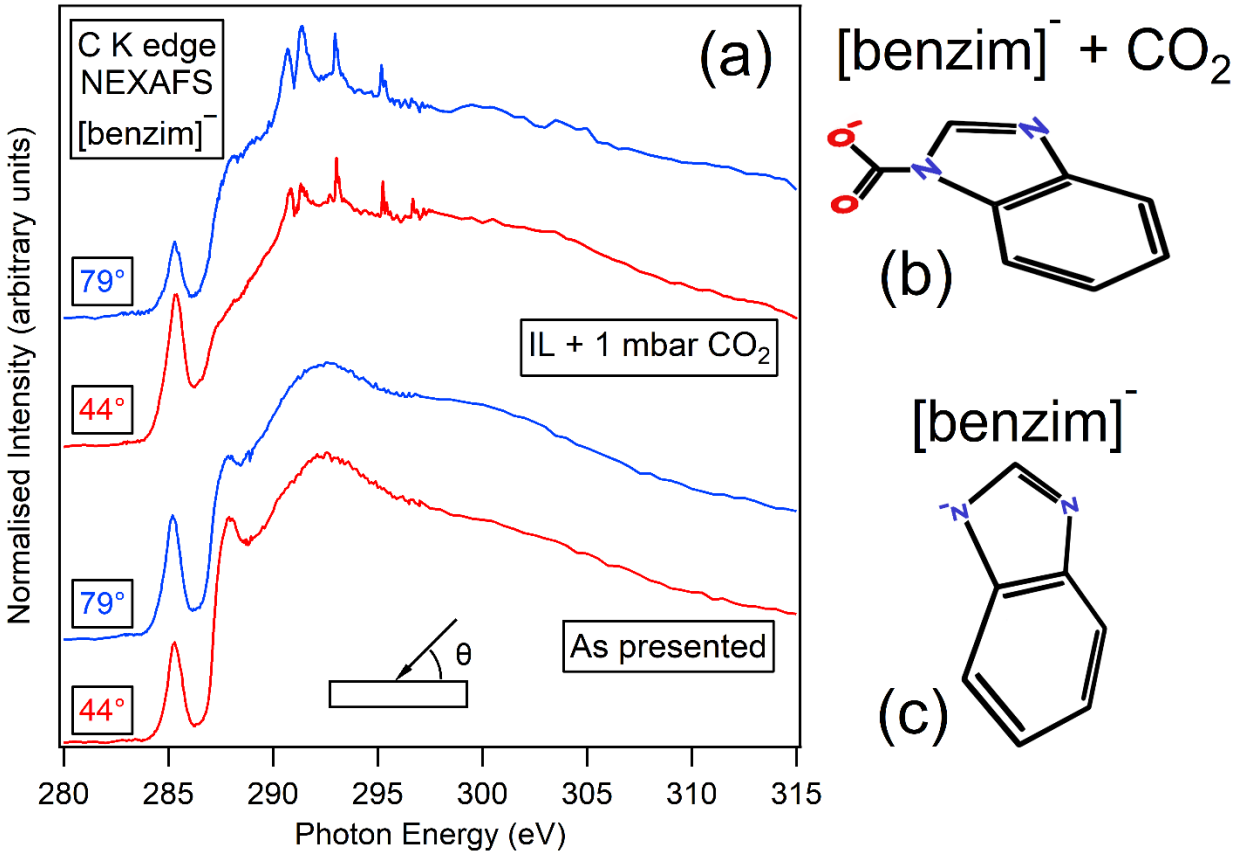

Figure 3. (a) C K edge NEXAFS spectra of $[P_{66614}][benzim]$ as presented and when exposed to 1 mbar of CO_2, for the X-ray beam incident at angles (θ) of 44° and 79° from the IL surface. Schematic pictures indicating the orientation of the anion (b) while exposed to CO_2 (benzim ring 54° from surface normal) and (c) as presented (benzim ring 27° from surface normal).

For the as presented IL, there is a split π* peak with two features at 285.3 and 287.9 eV, and a σ* peak at 292.6 eV. Walsh et al. found a split π* peak at similar photon energies over the C K

edge for benzimidazole on Cu (100) for multilayer coverage.[37] They also found that the higher-energy π* peak disappears at submonolayer coverage. Angle-resolved NEXAFS allows us to determine the orientation of the anion on the TiO_2 (110) substrate by comparing the relative intensities of the π* and σ* peaks at different X-ray angles of incidence. Relative to the σ* peak, the lower-energy π* peak at 285.3 eV is more intense for an X-ray incidence angle of 79° than for 44°. As π* orbitals point perpendicular out of the plane of the benzimidazolide ring, we can infer that the ring of the anion preferentially orients towards the surface normal (i.e. upright from the surface, as shown schematically in Figure 3(c)). We can estimate the tilt of the ring of the anion from the surface normal by calculating the intensity ratio of the lowest-energy π* peaks at both X-ray incidence angles and comparing them to the theoretical intensity ratio calculated using the Stöhr equations, assuming a random azimuthal orientation.[38] The benzim ring is oriented approximately 27° from the surface normal prior to CO_2 exposure (see Figure S17 in the SI).

Upon exposure to 1 mbar of CO_2, the lower-energy π* peak at 285.3 eV is significantly more intense relative to the σ* peak at approximately 291 eV for X-rays incident at 44° rather than 79°, indicating that benzim ring tends to lie closer to the plane of the substrate when exposed to CO_2 (approximately 54° from the surface normal, as shown in Figures 3(b) and S17).This suggests that the formation of carbamate at the anion induces a realignment of the IL at the TiO_2 surface. N K edge NEXAFS spectra (Figure S10) suggest further reorientation of the anions towards the surface with increasing CO_2 pressure. To the best of our knowledge, realignment of ions in ultrathin IL films upon absorption of CO_2 has not been previously reported.

DFT simulations were carried out and the simulated C K edge NEXAFS spectra were compared to experimental spectra as shown in Figure 4(a). For the IL as presented, the theoretical DFT spectrum has three π* peaks at 285.3, 287.6 and 290.3 eV, and a σ* peak at 293.2 eV. These

correspond to features in the experimental spectra at 285.3, 287.9, 290.2 (feature is very small) and 292.6 eV, respectively. As the DFT simulations are not angle-resolved, the intensities of these features are not comparable to those of the experimental data, only the positions of the features are comparable. In the DFT spectrum there is a slight broadening of the lowest energy π* peak towards higher photon energies, as shown in Figure S11.

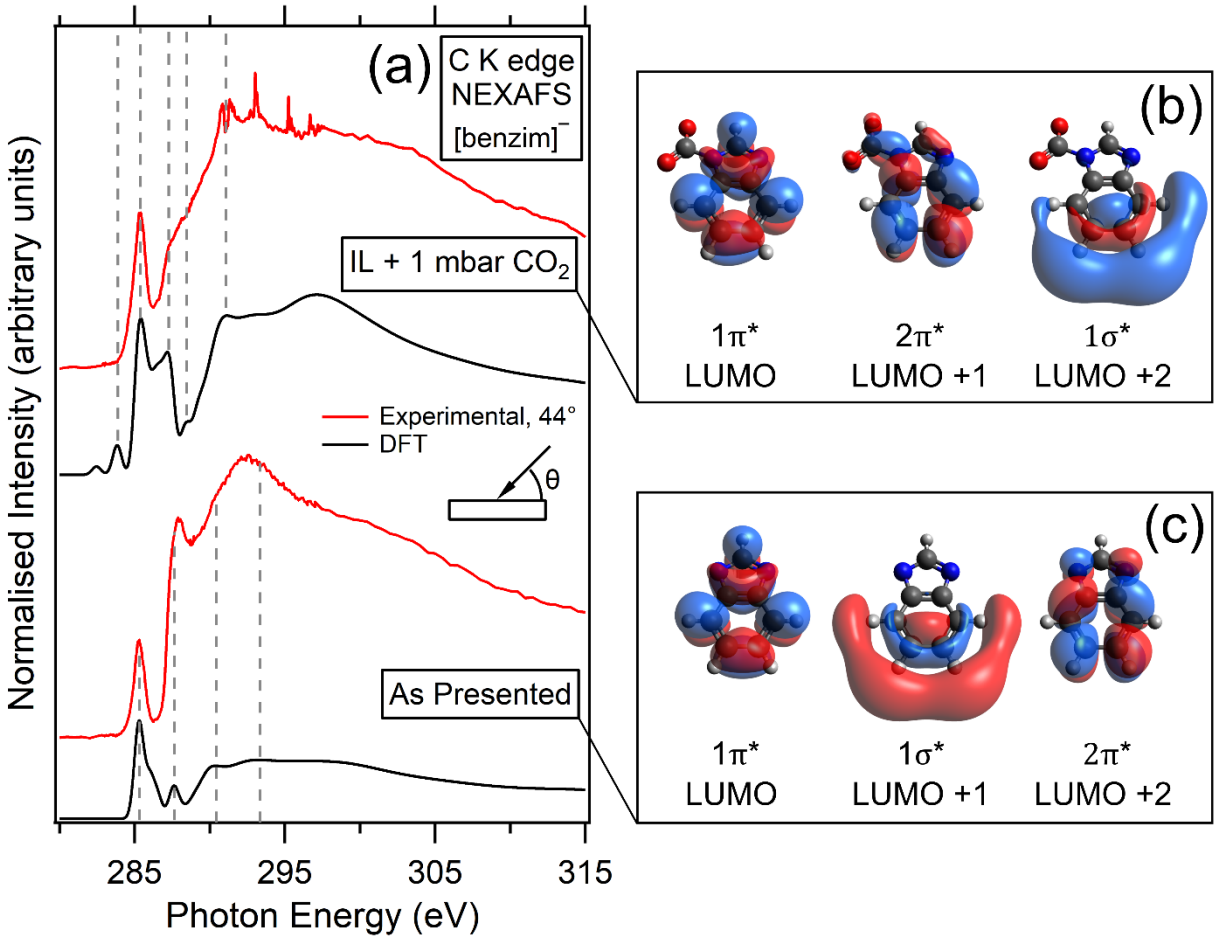

Figure 4. (a) Experimental and simulated (DFT) C K edge NEXAFS of $[P_{66614}][benzim]$ as presented and when exposed to 1 mbar of CO_2. The grey dashed lines highlight features of the DFT spectra for comparison with the experimental spectra. The experimental spectra were taken 44° from the IL surface. (b) Lowest unoccupied molecular orbitals (LUMOs) of $[benzim]^-$ + CO_2 arranged in order of increasing energy (left to right). LUMO, LUMO+1 and LUMO+2 are assigned

to the 1π*, 2π* and 1σ* antibonding orbitals, respectively. (c) LUMO, LUMO+1 and LUMO+2 of the isolated [benzim]$^-$ anion, assigned to the 1π*, 1σ* and 2π* antibonding orbitals, respectively.

When simulating the IL exposed to CO_2, the CO_2 was bonded to atom N^1 to form carbamate as shown in Figure 1(a). The negative charge from N^1 was given to the singly-bonded O atom. The IL + CO_2 DFT spectrum has three π* peaks at 285.3, 287.2 and 288.4 eV, and a σ* peak at 291.1 eV. These occur at the same energies as their corresponding peaks in the experimental spectra.

To complement the simulated NEXAFS spectra, unoccupied antibonding orbitals of the isolated and CO_2-reacted [benzim]$^-$ anion were computed using ORCA. This allows us to assign features of the experimental NEXAFS spectra to specific atoms in the anion. Figure 4(c) shows the lowest unoccupied molecular orbital (LUMO), LUMO+1, and LUMO+2 orbitals for [benzim]$^-$. These are similar to those of imidazole obtained by Thomason et al. and can be assigned as 1π*, 1σ* and 2π* orbitals, respectively.[39] The 1π* orbital shows four distinct environments of C atoms in the anion: $C^{1,2}$, $C^{3,6}$, $C^{4,5}$, C^7. This agrees with the simulated NEXAFS spectra of each individual atom in the [benzim]$^-$ anion in Figure S11, showing the same four environments. The π* peak at 285.3 eV (1π*) in the DFT spectrum is largely attributed to transitions from atoms $C^{3,6,7}$, while the 2π* peak at 287.6 eV is attributed to transitions from atom C^7. From this we can assign the π* peaks at 285.3 and 287.9 eV in the IL as presented experimental spectrum as $C^{3,6,7}$ → 1π* (LUMO) and C^7 → 2π* (LUMO+2) transitions, respectively. The C → 1σ* transition is weak and therefore cannot be resolved in this spectrum. Figure 4(b) shows the LUMO, LUMO+1 and LUMO+2 orbitals for the CO_2-reacted anion. When the anion reacts with CO_2, the π* peaks at 285.3 and 287.2 eV are assigned to $C^{1,2,3,6}$ → 1π* (LUMO) and $C^{4,5,7}$ → 2π* (LUMO+1) transitions, respectively. The DFT spectrum in Figure S12 shows that there is very little π* character on C^8 in the carbamate. This

may be a consequence of the way the negative charge was assigned in the simulations (as discussed in the SI).

Surface structure of IL thin and thick films has previously been explored using a variety of different substrates including metals (Au,[20,40] Ag,[41] Cu,[37,42] Pt[43]), metal oxides (TiO_2,[22,44] ZnO[45]), carbon (graphite,[46] graphene,[47] nanotubes[48]), and many more. We opted to study rutile TiO_2 (110) as our substrate for its relevance in a wide range of IL-based technologies including catalysts, TiO_2 nanotubes, and photovoltaic devices.[49–51] Modification of these systems using ILs can lead to greener technologies with improved performance and stability.[12,52,53]

Orientational ordering of ILs is typically demonstrated with imidazolium-based ions with long alkyl chains that preferentially orient towards the vacuum and away from the surface due to interactions at the IL/vacuum interface.[22,54] However, reordering of IL thin films upon absorption of CO_2 has not been shown experimentally prior to this study, to the best of our knowledge. Alternatively, some groups have carried out molecular dynamics simulations to investigate ordering of IL thin films on various solid surfaces,[55–58] and CO_2 absorption in bulk ILs.[59] It is clear that complementary computational and experimental studies are required to gain a deeper insight into the physical and chemical effects of reordering of IL films in realistic environments.

CONCLUSIONS

Absorption of CO_2 in a thin film of the IL $[P_{66614}]$[benzim] was studied using *in situ* near-ambient pressure X-ray photoelectron spectroscopy (NAP-XPS) and near edge X-ray absorption fine structure (NEXAFS). Results indicate that reaction with CO_2 leads to the formation of carbamate and causes a reordering of the cations and anions. The $[benzim]^-$ anions orient approximately 27° from the surface normal before exposure to CO_2 and approximately 54° from the surface normal when they react with CO_2. Angle-resolved XPS shows a greater concentration of CO_2-reacted

anions in the deeper layers of the ionic liquid. Additionally, there is evidence that the reaction with CO_2 is not fully reversible in our thin film. Experimental NEXAFS spectra are in good agreement with simulated NEXAFS spectra obtained using density functional theory. Unoccupied antibonding molecular orbitals were calculated and used to assign electron transitions to the spectral features of the experimental NEXAFS. CO_2-induced reordering of IL films may impact the performance of IL-based technologies such as photovoltaic devices, IL lubricants, and catalysis.

ASSOCIATED CONTENT

Supporting Information. *In situ* X-ray photoelectron spectra (survey, Ti 2p, grazing emission study of C 1s and O 1s) of the ionic liquid $[P_{66614}]$[benzim] taken at ultra-high vacuum and while exposed to increasing pressures of CO_2 up to 5 mbar, and near edge X-ray absorption fine structure spectra (experimental CO_2 background gas correction, DFT simulations).

AUTHOR INFORMATION

Corresponding Authors

*Email: KSyres@uclan.ac.uk; JCole4@uclan.ac.uk

Present Addresses

Department of Chemistry and Henry Royce Institute, University of Manchester, Manchester, M13 9PL, UK

⊥ Helmholtz-Zentrum Berlin für Materialien und Energie, Berlin, Germany.

ACKNOWLEDGMENT

We acknowledge Diamond Light Source for time on Beamline B07-VERSOX under Proposal SI-20532. The authors acknowledge the Jeremiah Horrocks Institute for the PhD studentships for Zoë Henderson and Jordan Cole, and Mexican Institutions CONACYT/ SENER for the PhD scholarship support for Claudia Lorena Compeán González No 472709.

ABBREVIATIONS

NEXAFS, near edge X-ray absorption fine structure; NAP-XPS, near-ambient pressure X-ray photoelectron spectroscopy; MEA, monoethanolamine, SBIL, superbasic ionic liquid; $[P_{66614}]$[benzim], trihexyltetradecylphosphonium benzimidazolide.

REFERENCES

(1) Boot-Handford, M. E.; Abanades, J. C.; Anthony, E. J.; Blunt, M. J.; Brandani, S.; Mac Dowell, N.; Fernández, J. R.; Ferrari, M. C.; Gross, R.; Hallett, J. P.; et al. Carbon Capture and Storage Update. *Energy Environ. Sci.* **2014**, *7*, 130–189.

(2) Yu, C. H.; Huang, C. H.; Tan, C. S. A Review of CO_2 Capture by Absorption and Adsorption. *Aerosol Air Qual. Res.* **2012**, *12*, 745–769.

(3) Cuéllar-Franca, R. M.; García-Gutiérrez, P.; Taylor, S. F. R.; Hardacre, C.; Azapagic, A. A Novel Methodology for Assessing the Environmental Sustainability of Ionic Liquids Used for CO_2 Capture. *Faraday Discuss.* **2016**, *192*, 283–301.

(4) Bates, E. D.; Mayton, R. D.; Ntai, I.; Davis, J. H. CO_2 Capture by a Task-Specific Ionic Liquid. *J. Am. Chem. Soc.* **2002**, *124*, 926–927.

(5) Welton, T. Ionic Liquids: A Brief History. *Biophys. Rev.* **2018**, *10*, 691–706.

(6) Guo, F.; Zhang, S.; Wang, J.; Teng, B.; Zhang, T.; Fan, M. Synthesis and Applications of Ionic Liquids in Clean Energy and Environment: A Review. *Curr. Org. Chem.* **2015**, *19*, 455–468.

(7) Mumford, K. A.; Wu, Y.; Smith, K. H.; Stevens, G. W. Review of Solvent Based Carbon-Dioxide Capture Technologies. *Front. Chem. Sci. Eng.* **2015**, *9*, 125–141.

(8) Li, H.; Qu, J.; Cui, Q.; Xu, H.; Luo, H.; Chi, M.; Meisner, R. A.; Wang, W.; Dai, S. TiO_2 Nanotube Arrays Grown in Ionic Liquids: High-Efficiency in Photocatalysis and Pore-Widening. *J. Mater. Chem.* **2011**, *21*, 9487–9490.

(9) Li, X.; Zhao, Z.; Pan, C. Ionic Liquid-Assisted Electrochemical Exfoliation of Carbon Dots of Different Size for Fluorescent Imaging of Bacteria by Tuning the Water Fraction in Electrolyte. *Microchim. Acta* **2016**, *183*, 2525–2532.

(10) Macfarlane, D. R.; Tachikawa, N.; Forsyth, M.; Pringle, J. M.; Howlett, P. C.; Elliott, G. D.; Davis, J. H.; Watanabe, M.; Simon, P.; Angell, C. A. Energy Applications of Ionic Liquids. *Energy Environ. Sci.* **2014**, *7*, 232–250.

(11) Roy, P.; Kim, D.; Lee, K.; Spiecker, E.; Schmuki, P. TiO_2 Nanotubes and Their Application in Dye-Sensitized Solar Cells. *Nanoscale* **2010**, *2*, 45–59.

(12) Bai, S.; Da, P.; Li, C.; Wang, Z.; Yuan, Z.; Fu, F.; Kawecki, M.; Liu, X.; Sakai, N.; Wang, J. T.; et al. Planar Perovskite Solar Cells with Long-Term Stability Using Ionic Liquid Additives. *Nature* **2019**, *571*, 245–250.

(13) Li, C.; Lu, D.; Wu, C. The Role of Cations in the Interactions between Anionic N-Heterocycles and SO_2. *Sci. Rep.* **2018**, *8*, 1–9.

(14) Greer, A. J.; Jacquemin, J.; Hardacre, C. Industrial Applications of Ionic Liquids. *Molecules* **2020**, *25*, 1–31.

(15) Wang, C.; Luo, X.; Luo, H.; Jiang, D.; Li, H.; Dai, S. Tuning the Basicity of Ionic Liquids for Equimolar CO_2 Capture. *Angew. Chemie* **2011**, *123*, 5020–5024.

(16) Greer, A. J.; Taylor, S. F. R.; Daly, H.; Quesne, M.; Catlow, C. R. A.; Jacquemin, J.; Hardacre, C. Investigating the Effect of NO on the Capture of CO_2 Using Superbase Ionic Liquids for Flue Gas Applications. *ACS Sustain. Chem. Eng.* **2019**, *7*, 3567–3574.

(17) Taylor, S. F. R.; McCrellis, C.; McStay, C.; Jacquemin, J.; Hardacre, C.; Mercy, M.; Bell, R. G.; De Leeuw, N. H. CO_2 Capture in Wet and Dry Superbase Ionic Liquids. *J. Solution Chem.* **2015**, *44*, 511–527.

(18) Cremer, T.; Killian, M.; Gottfried, J. M.; Paape, N.; Wasserscheid, P.; Maier, F.; Steinrück, H. P. Physical Vapor Deposition of [EMIM][Tf_2N]: A New Approach to the Modification of Surface Properties with Ultrathin Ionic Liquid Films. *ChemPhysChem* **2008**, *9*, 2185–2190.

(19) Deyko, A.; Cremer, T.; Rietzler, F.; Perkin, S.; Crowhurst, L.; Welton, T.; Steinrück, H. P.; Maier, F. Interfacial Behavior of Thin Ionic Liquid Films on Mica. *J. Phys. Chem. C* **2013**, *117*, 5101–5111.

(20) Cremer, T.; Stark, M.; Deyko, A.; Steinrück, H. P.; Maier, F. Liquid/Solid Interface of Ultrathin Ionic Liquid Films: [C_1C_1Im][Tf_2N] and [C_8C_1Im][Tf_2N] on Au(111). *Langmuir* **2011**, *27*, 3662–3671.

(21) Cremer, T.; Wibmer, L.; Calderón, S. K.; Deyko, A.; Maier, F.; Steinrück, H. P. Interfaces of Ionic Liquids and Transition Metal Surfaces - Adsorption, Growth, and Thermal Reactions of Ultrathin $[C_1C_1Im][Tf_2N]$ Films on Metallic and Oxidised Ni(111) Surfaces. *Phys. Chem. Chem. Phys.* **2012**, *14*, 5153–5163.

(22) Wagstaffe, M.; Jackman, M. J.; Syres, K. L.; Generalov, A.; Thomas, A. G. Ionic Liquid Ordering at an Oxide Surface. *ChemPhysChem* **2016**, *17*, 3430–3434.

(23) Held, G.; Venturini, F.; Grinter, D. C.; Ferrer, P.; Arrigo, R.; Deacon, L.; Garzon, W. Q.; Roy, K.; Large, A.; Stephens, C.; et al. Ambient-Pressure Endstation of the Versatile Soft X-Ray (VerSoX) Beamline at Diamond Light Source. *J. Synchrotron Radiat.* **2020**, *27*, 1153–1166.

(24) Bradaric, C. J.; Downard, A.; Kennedy, C.; Robertson, A. J.; Zhou, Y. Industrial Preparation of Phosphonium Ionic Liquids. *Green Chem.* **2003**, *5*, 143–152.

(25) Fairely, N. *CasaXPS*. Casa Software Ltd.: Teignmouth, Devon, 2009.

(26) Blundell, R. K.; Licence, P. Quaternary Ammonium and Phosphonium Based Ionic Liquids: A Comparison of Common Anions. *Phys. Chem. Chem. Phys.* **2014**, *16*, 15278–15288.

(27) Hermann, K.; Pettersson, L. G. M.; Casida, M. E.; Daul, C.; Goursot, A.; Koester, A.; Proynov, E.; St-Amant, A.; Salahub, D. R.; Carravetta, V.; et al. *StoBe-DeMon 3.3*, StoBe Software, 2014.

(28) Hanwell, M. D.; Curtis, D. E.; Lonie, D. C.; Vandermeerschd, T.; Zurek, E.; Hutchison, G. R. Avogadro: An Advanced Semantic Chemical Editor, Visualization, and Analysis Platform. *J. Cheminform.* **2012**, *4*, 1–17.

(29) Diller, K.; Maurer, R. J.; Müller, M.; Reuter, K. Interpretation of X-Ray Absorption Spectroscopy in the Presence of Surface Hybridization. *J. Chem. Phys.* **2017**, *146*, 1–6.

(30) Neese, F. The ORCA Program System. *Wiley Interdiscip. Rev. Comput. Mol. Sci.* **2012**, *2*, 73–78.

(31) Neese, F. Software Update: The ORCA Program System, Version 4.0. *Wiley Interdiscip. Rev. Comput. Mol. Sci.* **2018**, *8*, 4–9.

(32) Villar-Garcia, I. J.; Smith, E. F.; Taylor, A. W.; Qiu, F.; Lovelock, K. R. J.; Jones, R. G.; Licence, P. Charging of Ionic Liquid Surfaces under X-Ray Irradiation: The Measurement of Absolute Binding Energies by XPS. *Phys. Chem. Chem. Phys.* **2011**, *13*, 2797–2808.

(33) Henderson, Z.; Thomas, A. G.; Wagstaffe, M.; Taylor, S. F. R.; Hardacre, C.; Syres, K. L. Reversible Reaction of CO_2 with Superbasic Ionic Liquid $[P_{66614}]$[Benzim] Studied with in Situ Photoelectron Spectroscopy. *J. Phys. Chem. C* **2019**, *123*, 7134–7141.

(34) Lovelock, K. R. J.; Smith, E. F.; Deyko, A.; Villar-Garcia, I. J.; Licence, P.; Jones, R. G. Water Adsorption on a Liquid Surface. *Chem. Commun.* **2007**, 4866–4868.

(35) Lewis, T.; Faubel, M.; Winter, B.; Hemminger, J. C. CO_2 Capture in Amine-Based Aqueous Solution: Role of the Gas-Solution Interface. *Angew. Chemie - Int. Ed.* **2011**, *50*, 10178–10181.

(36) Yerushalmi, R.; Ho, J. C.; Fan, Z.; Javey, A. Phosphine Oxide Monolayers on SiO_2 Surfaces. *Angew. Chemie - Int. Ed.* **2008**, *47*, 4440–4442.

(37) Walsh, J. F.; Dhariwal, H. S.; Gutiérrez-Sosa, A.; Finetti, P.; Muryn, C. A.; Brookes, N. B.; Oldman, R. J.; Thornton, G. Probing Molecular Orientation in Corrosion Inhibition via a

NEXAFS Study of Benzotriazole and Related Molecules on Cu(100). *Surf. Sci.* **1998**, *415*, 423–432.

(38) Stöhr, J. *NEXAFS Spectroscopy*; Springer: Berlin, 2003.

(39) Thomason, M. J.; Seabourne, C. R.; Sattelle, B. M.; Hembury, G. A.; Stevens, J. S.; Scott, A. J.; Aziz, E. F.; Schroeder, S. L. M. Self-Association of Organic Solutes in Solution: A NEXAFS Study of Aqueous Imidazole. *Faraday Discuss.* **2015**, *179*, 269–289.

(40) Grillo, F.; Garrido Torres, J. A.; Treanor, M. J.; Larrea, C. R.; Götze, J. P.; Lacovig, P.; Früchtl, H. A.; Schaub, R.; Richardson, N. V. Two-Dimensional Self-Assembly of Benzotriazole on an Inert Substrate. *Nanoscale* **2016**, *8*, 9167–9177.

(41) Buchner, F.; Forster-Tonigold, K.; Uhl, B.; Alwast, D.; Wagner, N.; Farkhondeh, H.; Groß, A.; Behm, R. J. Toward the Microscopic Identification of Anions and Cations at the Ionic Liquid|Ag(111) Interface: A Combined Experimental and Theoretical Investigation. *ACS Nano* **2013**, *7*, 7773–7784.

(42) Syres, K. L.; Jones, R. G. Adsorption, Desorption, and Reaction of 1-Octyl-3-Methylimidazolium Tetrafluoroborate, $[C_8C_1Im][BF_4]$, Ionic Liquid Multilayers on Cu(111). *Langmuir* **2015**, *31*, 9799–9808.

(43) Baldelli, S. Surface Structure at the Ionic Liquid−electrified Metal Interface. *Acc. Chem. Res.* **2008**, *41*, 421–431.

(44) Henderson, Z.; Walton, A. S.; Thomas, A. G.; Syres, K. L. Water-Induced Reordering in Ultrathin Ionic Liquid Films. *J. Phys. Condens. Matter* **2018**, *30*, No. 334003.

(45) Lee, B. R.; Choi, H.; Sunpark, J.; Lee, H. J.; Kim, S. O.; Kim, J. Y.; Song, M. H. Surface Modification of Metal Oxide Using Ionic Liquid Molecules in Hybrid Organic-Inorganic Optoelectronic Devices. *J. Mater. Chem.* **2011**, *21*, 2051–2053.

(46) Wang, S.; Li, S.; Cao, Z.; Yan, T. Molecular Dynamic Simulations of Ionic Liquids at Graphite Surface. *J. Phys. Chem. C* **2010**, *114*, 990–995.

(47) Fedorov, M. V.; Lynden-Bell, R. M. Probing the Neutral Graphene-Ionic Liquid Interface: Insights from Molecular Dynamics Simulations. *Phys. Chem. Chem. Phys.* **2012**, *14*, 2552–2556.

(48) Dong, K.; Zhou, G.; Liu, X.; Yao, X.; Zhang, S.; Lyubartsev, A. Structural Evidence for the Ordered Crystallites of Ionic Liquid in Confined Carbon Nanotubes. *J. Phys. Chem. C* **2009**, *113*, 10013–10020.

(49) Smiglak, M.; Pringle, J. M.; Lu, X.; Han, L.; Zhang, S.; Gao, H.; Mac Farlane, D. R.; Rogers, R. D. Ionic Liquids for Energy, Materials, and Medicine. *Chem. Commun.* **2014**, *50*, 9228–9250.

(50) Paramasivam, I.; Macak, J. M.; Selvam, T.; Schmuki, P. Electrochemical Synthesis of Self-Organized TiO_2 Nanotubular Structures Using an Ionic Liquid (BMIM-BF_4). *Electrochim. Acta* **2008**, *54*, 643–648.

(51) Park, N. G. Perovskite Solar Cells: An Emerging Photovoltaic Technology. *Mater. Today* **2015**, *18*, 65–72.

(52) Gorlov, M.; Kloo, L. Ionic Liquid Electrolytes for Dye-Sensitized Solar Cells. *J. Chem. Soc. Dalt. Trans.* **2008**, 2655–2666.

(53) Sowmiah, S.; Srinivasadesikan, V.; Tseng, M. C.; Chu, Y. H. On the Chemical Stabilities of Ionic Liquids. *Molecules* **2009**, *14*, 3780–3813.

(54) Lockett, V.; Sedev, R.; Bassell, C.; Ralston, J. Angle-Resolved X-Ray Photoelectron Spectroscopy of the Surface of Imidazolium Ionic Liquids. *Phys. Chem. Chem. Phys.* **2008**, *10*, 1330–1335.

(55) Shimizu, K.; Pensado, A.; Malfreyt, P.; Pádua, A. A. H.; Canongia Lopes, J. N. 2D or Not 2D: Structural and Charge Ordering at the Solid-Liquid Interface of the 1-(2-Hydroxyethyl)-3-Methylimidazolium Tetrafluoroborate Ionic Liquid. *Faraday Discuss.* **2012**, *154*, 155–169.

(56) Dragoni, D.; Manini, N.; Ballone, P. Interfacial Layering of a Room-Temperature Ionic Liquid Thin Film on Mica: A Computational Investigation. *ChemPhysChem* **2012**, *13*, 1772–1780.

(57) Kislenko, S. A.; Samoylov, I. S.; Amirov, R. H. Molecular Dynamics Simulation of the Electrochemical Interface between a Graphite Surface and the Ionic Liquid [BMIM][PF_6]. *Phys. Chem. Chem. Phys.* **2009**, *11*, 5584–5590.

(58) Liu, L.; Li, S.; Cao, Z.; Peng, Y.; Li, G.; Yan, T.; Gao, X. P. Well-Ordered Structure at Ionic Liquid/Rutile (110) Interface. *J. Phys. Chem. C* **2007**, *111*, 12161–12164.

(59) Zhang, X.; Zhang, X.; Dong, H.; Zhao, Z.; Zhang, S.; Huang, Y. Carbon Capture with Ionic Liquids: Overview and Progress. *Energy Environ. Sci.* **2012**, *5*, 6668–6681.

TOC GRAPHIC

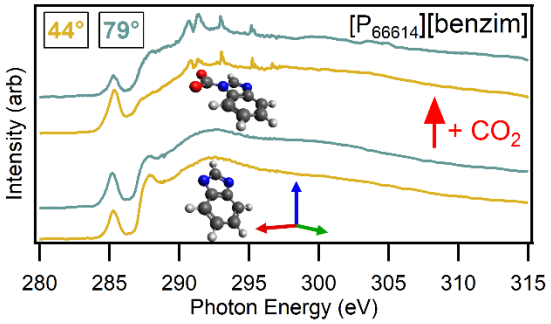
44°
79°
[P66614][benzim]
+ CO2
Intensity (arb)
280
285
290
295
300
305
310
315
Photon Energy (eV)